

Transport properties of nonhomogeneous segregated composites

B. Nigro,^{1,*} G. Ambrosetti,¹ C. Grimaldi,^{1,†} T. Maeder,¹ and P. Ryser¹

¹*LPM, Ecole Polytechnique Fédérale de Lausanne, Station 17, CP-1015 Lausanne, Switzerland*

In conductor-insulator composites in which the conducting particles are dispersed in an insulating continuous matrix the electrical connectedness is established by interparticle quantum tunneling. A recent formulation of the transport problem in this kind of composites treats each conducting particle as electrically connected to all others via tunneling conductances to form a global tunneling network. Here, we extend this approach to nonhomogeneous composites with a segregated distribution of the conducting phase. We consider a model of segregation in which large random insulating spherical inclusions forbid small conducting particles to occupy homogeneously the volume of the composite, and allow tunneling between all pairs of the conducting objects. By solving numerically the corresponding tunneling resistor network, we show that the composite conductivity σ is enhanced by segregation and that it may remain relatively large also for very small values of the conducting filler concentration. We interpret this behavior by a segregation-induced reduction of the interparticle distances, which is confirmed by a critical path approximation applied to the segregated network. Furthermore, we identify an approximate but accurate scaling relation permitting to express the conductivity of a segregated systems in terms of the interparticle distances of a corresponding homogeneous system, and which provides an explicit formula for σ which we apply to experimental data on segregated RuO₂-cermet composites.

PACS numbers: 64.60.ah, 73.40.Gk, 72.80.Tm, 72.20.Fr

I. INTRODUCTION

The transport properties of two-phase heterogeneous materials are strongly related to the structure of the composite i.e. the volume fraction ϕ of the conductive fillers, their size and shape, and their dispersion into the insulating medium.^{1,2} Controlling the conductivity σ of disordered composite materials by tuning these structural parameters is of fundamental importance for several applications in the fields of micro and nanoelectronics such as, to name a few, electromagnetic interference shielders, resectable fuses, strain and chemical sensors, flexible conductors, and anti-static compounds.³

In several classes of composite materials in which the conductive particles are dispersed into a insulating medium, like e.g. polymer-based composites or metal-glass cermets, the prominent transport mechanism is quantum tunneling. In this case of tunneling, the conductance between two particles decays exponentially with the inter-particle distance over a characteristic tunneling length ξ which is of the order of a fraction to a few nanometers depending on the material characteristics.

Typically, the tunneling mechanism is approximated by treating the fillers as core-shell objects, where the impenetrable hard core represents the physical particle and the thickness of the concentric penetrable shell is identified with $\sim \xi$.⁴⁻⁷ In this way, the overall behavior of the composite conductivity σ as a function of ϕ is commonly interpreted in the framework of percolation theory,^{8,9} which considers two given conducting particles as either electrically connected or disconnected if their mutual distance is respectively lower or larger than the cut-off length imposed by the shell thickness. Under this assumption, the system undergoes a conductor-insulator transition at a critical concentration ϕ_c of conducting

phase, which is associated with the formation of a globally connected cluster of electrically linked filler particles which spans the entire sample. Below ϕ_c there is no such sample-spanning cluster and σ is zero, while for $\phi > \phi_c$ the conductivity follows a power law behavior of the form $\sigma \propto (\phi - \phi_c)^t$, where t is a critical exponent.

Despite of its simplicity and of the unquestionable insights that it provides on the transport problem,¹⁰⁻¹³ introducing the concept of a cut-off through which electrical connections are established, is nevertheless a too crude approximation which alters the real nature of the interparticle electrical connectedness. This is indeed characterized by the fact that, due to the tunneling mechanism, two given particles are always electrically connected regardless of their mutual distance,¹⁴ even if the strength of the connection (i.e., the interparticle conductance) decays exponentially with such distance.

Recently, we have reformulated the transport problem in conductor-insulator composites by allowing each conducting particle to be connected to all others via tunneling processes,¹⁵⁻¹⁷ and so without imposing the restrictive hypothesis on which the usual core-shell model is based. By explicitly taking into account the composite morphology or microstructure and the conducting particles shape and dimensions, this global tunneling network (GTN) model is able to describe the overall conductivity dependence upon the particle concentration for many different classes of composites, ranging from granular-like systems to colloidal dispersions in a continuum insulating matrix.¹⁷ When applied to the many published data on colloidal nanotube, nanofiber, nanosheets, and nanosphere composites, this formalism has permitted to extract important microscopic properties, such as the tunneling decay length ξ , directly from the experimental conductivity vs concentration curves.^{15,16}

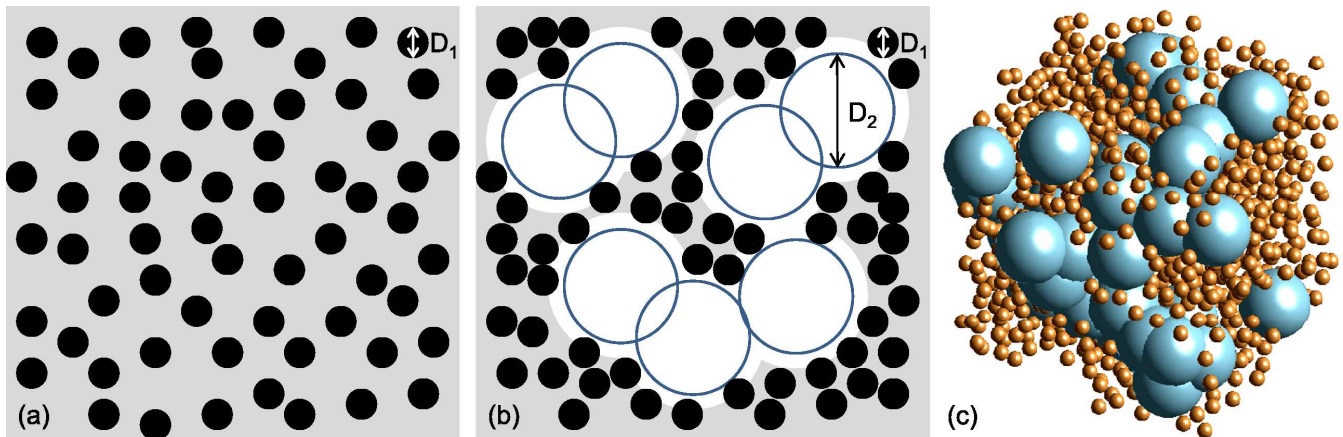


FIG. 1: (Color online) Two-dimensional representation of (a) an homogeneous and (b) segregated dispersion of the conducting particles in the continuum. The insulating (conducting) inclusions are represented by open (filled) circles of diameter D_2 (D_1). The insulating fillers can penetrate each other, while the conducting particles are impenetrable with respect to themselves and to the insulating ones. The grey region represents the space available for placing the centers of the conducting spheres. (b) Example of a distribution of insulating and conducting particles with $D_2/D_1 = 4$.

In this paper we apply the GTN model to composites where the dispersion of the conducting fillers in the insulating continuum is not homogeneous. Specifically, we consider systems in which the insulating phase forbids the conducting fillers to occupy large (compared to the particle size) volumes inside the material, thereby leading to a segregated spatial distribution of the conducting phase.^{6,18,19} In real composites, like e.g. RuO₂-based cermets,²⁰ this is achieved when the size of the insulating grains is consistently larger than the one of the conducting fillers, and thermal treatments, inducing softening and sintering of the insulating phase without large-scale mixing, lead to a segregated distribution of the conducting particles in a continuous insulating matrix. Besides the already cited RuO₂-based cermets, another important class of segregated conductive composites is that of polymer-based ones,^{21,22} where an inorganic or carbonaceous conductive filler is mixed with significantly larger polymer particles and the resulting compound is molded.

The study of the transport properties in segregated composites is important for many technological applications where low filler concentrations are demanded in order to have high conduction regimes combined with the unaltered mechanical properties of the host insulating medium, or to reduce the quantity of the conductive phase when its cost is high. So far, the problem of conduction in segregated systems has been limited to the evaluation of the critical concentration ϕ_c within the percolation framework, and both lattice^{18,21,23} and continuum^{6,19} models have evidenced that ϕ_c is (usually, see Ref.19) lowered by segregation. In the following we shall go beyond the percolation approach by considering the GTN scenario for the segregation problem and by solving numerically the tunneling network equations. We find that the composite conductivity σ for fixed filler

concentration can be strongly enhanced by the segregation, in accord with the observed trends. Furthermore, we show that the calculated filler dependencies of σ can be reproduced to a great accuracy by the critical path approximation,²⁴ which we find to follow a simple scaling law permitting us to provide analytical formulas for $\sigma(\phi)$. When applied to experimental data of real segregated composites, our formulas can be used to estimate the degree of segregation of the composite and the value of the tunneling length ξ .

The structure of the paper is as follows: in Sec. II we present our GTN model for segregated composites and in Sec. III we calculate numerically the composite conductivities. In Sec. IV we present our results on the critical tunneling distance which will be used to approximate the numerical results of Sec. III and to provide explicit formulas for the conductivity. These are applied in Sec. V to some previously published data of segregated composites to extract the tunneling distance. Section VI is left to the conclusions.

II. MODEL

We model the conductor-insulator composite as described in Fig. 1(a) and (b) for the case of an homogeneous dispersions of conducting particles in the continuum and for a segregated distribution, respectively. In Fig. 1(b) the spherical particles of diameter D_2 represent the insulating inclusions (e.g., the glassy frit particles in RuO₂ cermets) while the conducting particles are modeled as hard spheres of diameter D_1 . The two kinds of particles are mutually impenetrable and, furthermore, we assume that the D_2 spheres can penetrate each other in order to simulate for instance sintering and softening of

the insulating grains. Typically, as in RuO₂ cermets, D_2 is as large as a few micrometers while D_1 ranges from tens to hundreds of nanometers, so that the regime $D_2 \gg D_1$ is the one of practical interest. Keeping this in mind, we shall consider in the following also moderate values of D_2/D_1 to better appreciate the overall trends towards the $D_2/D_1 \gg 1$ regime.

The system is generated by first randomly placing the penetrable insulating spheres into a three dimensional cubic volume of side length L with a given number density $\rho_2 = N_2/L^3$, where N_2 is the number of D_2 particles and L is chosen to be at least one order of magnitude larger than D_2 (we assume periodic boundary conditions). Since the positions of the insulating spheres are uncorrelated, their fractional volume is $\phi_2 = 1 - \exp(-v_2\rho_2)$ where $v_2 = \pi D_2^3/6$ is the volume of a single sphere.²⁵ After having placed the insulating spheres, N_1 conducting hard spheres are added to the system through random sequential addition (RSA), where random placing is accepted only if there is no overlap with the other D_1 and D_2 spheres. The RSA procedure is repeated until the desired volume fraction value $\phi_1 = \rho_1 v_1$, where $v_1 = \pi D_1^3/6$ and $\rho_1 = N_1/L^3$, is reached. However, since the conducting spheres cannot penetrate the insulating ones, the available volume for placing the centers of the D_1 particles is reduced by the factor¹⁹

$$v^* = (1 - \phi_2)^{(1+D_1/D_2)^3} \quad (1)$$

with respect to the total volume L^3 of the system. This defines an effective volume fraction ϕ_1/v^* , larger than ϕ_1 , for the conducting spheres. Hence, for small values of v^* , the limit achievable through RSA can become much lower than that of the homogeneous limit at $v^* = 1$, which is $\phi_1^{\max} \simeq 0.382$,²⁶ and scales approximately as $\phi_1^{\max} v^*$. For densities larger than the RSA limit we have considered cubically arranged initial configurations where particles overlapping with the insulating spheres were removed. Both the initial RSA and the cubic configurations were then relaxed via Monte Carlo runs, where random displacements of the D_1 sphere centers were attempted and accepted only if they did not overlap with any of its neighbors and with the D_2 particles. Equilibrium was considered attained when the mean nearest-neighbor distances between the D_1 particles did not change within statistical errors upon further Monte Carlo displacements. An example of the so-obtained distribution of D_1 and D_2 spheres is shown in Fig. 1(b) for the case $D_2/D_1 = 4$.

In describing the overall conductivity arising from the system described above we go beyond the usual core-shell approximation, and employ the GTN model to the subset of D_1 particles of the composite. Hence, we treat any two conducting spheres centered at \mathbf{r}_i and \mathbf{r}_j as electrically connected through tunneling processes, irrespectively of their mutual distance $r_{ij} = |\mathbf{r}_i - \mathbf{r}_j|$. By assuming that the particle size D_1 and the temperature are large enough to neglect charging energy effects, then the inter-particle

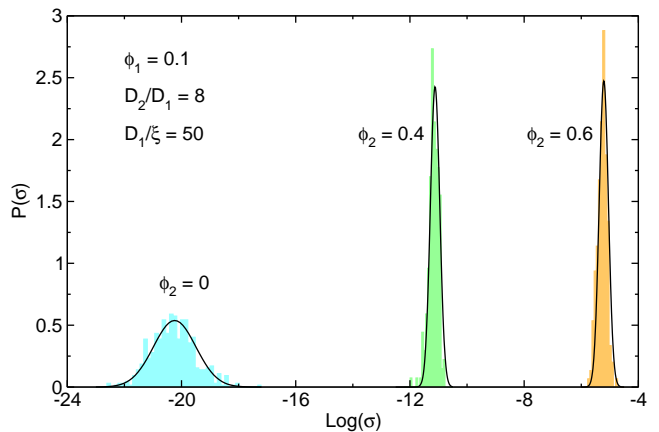


FIG. 2: (Color online) Histograms for the distribution $P(\sigma)$ of the conductivity obtained from 500 realizations of the tunneling network for $D_2/D_1 = 8$, $D_1/\xi = 50$ and $\phi_1 = 0.1$. The volume fraction values of the insulating spheres are $\phi_2 = 0$ (with $L/D_1 = 25$) and $\phi_2 = 0.4, 0.6$ (with $L/D_1 = 80$). The solid lines are fits to log-normal distribution functions.

conductance is given by:

$$g_{ij} = g_0 \exp\left(-\frac{2\delta_{ij}}{\xi}\right) \quad (2)$$

where g_0 is a constant “contact” conductance which we shall set equal to the unity, ξ is the tunneling decay length, and $\delta_{ij} = r_{ij} - D_1$ is the minimal distance between the surfaces of two conducting spheres. For a system composed by N_1 particles, the GTN model is then equivalent to a weighted random network with N_1 nodes, each with coordination number $N_1 - 1$. However, contrary to the usual models of weighted networks,²⁷ the weight of each link is not random but it is given by Eq. (2), which depends on the particular arrangement of the conducting fillers in the composite. This characteristics of the model permits in principle to study on equal footing composites with different statistical properties of the microstructure, and has been successfully applied to homogeneous colloidal and granular composites.^{15–17} In the following we shall show that the GTN approach is also able to describe the conductivity of segregated systems, thus providing a theoretical framework for the study of inhomogeneous composites.

III. CONDUCTIVITY

In this section we present the results of our numerical calculations of the filler concentration dependence of the conductivity σ for different segregated systems specified by ϕ_2 and D_2/D_1 . Since in the GTN model each conducting particle is connected to all others through Eq. (2), the calculation of σ would require the solution of a network with $N_1(N_1 - 1)/2$ resistors, which is a computationally

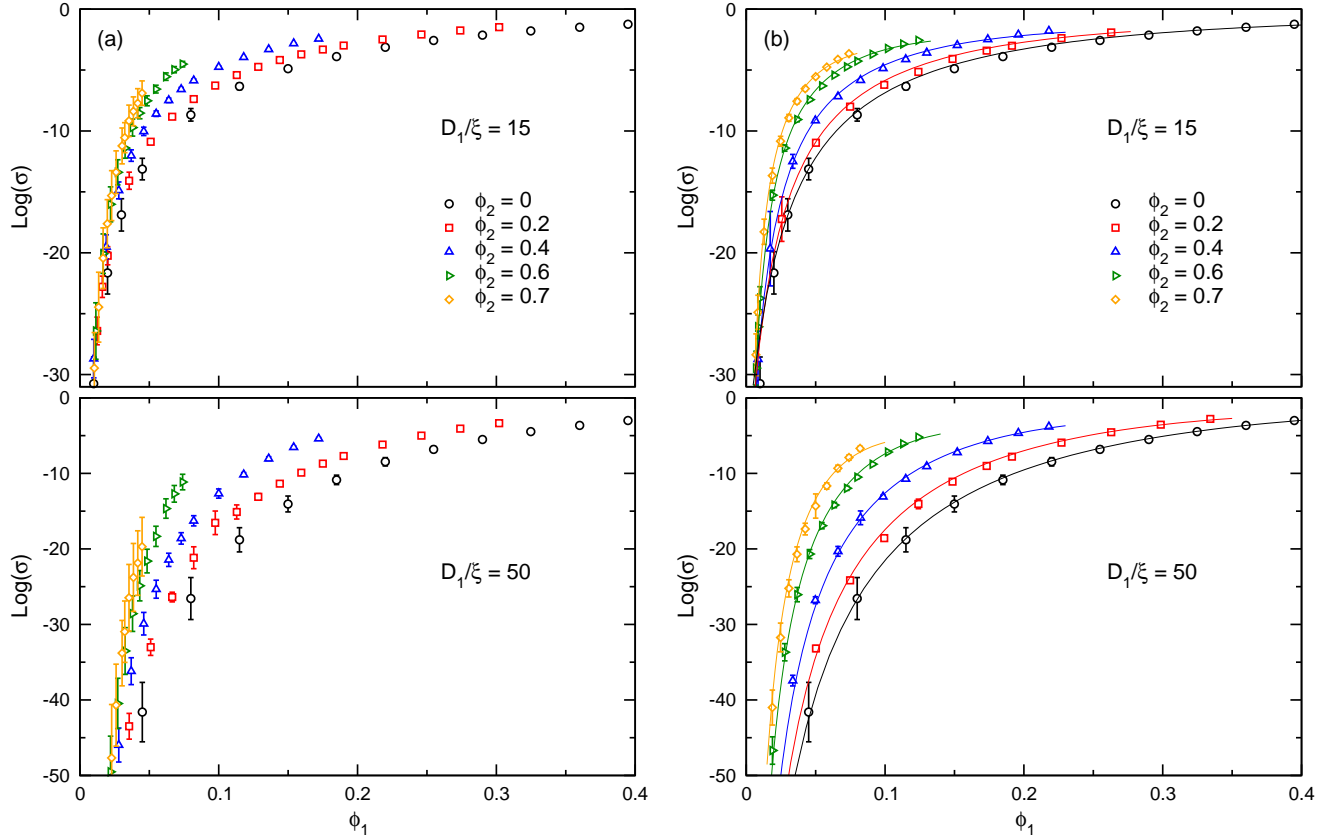


FIG. 3: (Color online) Calculated GTN conductivity as a function of the volume fraction ϕ_1 of the conducting spheres with diameter D_1 for $D_1/\xi = 15$ and 50, and for different values of the volume fraction ϕ_2 of the insulating spheres with diameter D_2 . (a) $D_2/D_1 = 4$, (b) $D_2/D_1 = 8$. The solid lines in (b) are fits of our formula.

demanding, or even insurmountable, task for the N_1 values considered in our study. However, we can exploit the exponential decay of Eq. (2) by neglecting contributions from tunneling between particles sufficiently far away apart. Indeed, depending on the value of ξ and of the filler concentration ϕ_1 , it is possible to identify an upper artificial cut-off δ^* such that the conductances between particles at mutual distances $\delta_{ij} > \delta^*$ can be safely removed, reducing drastically the number of connected particles in the network. In our calculations we have then chosen δ^* such that, depending on ϕ_1 , $\exp(-2\delta^*/\xi)$ is from five to twenty orders of magnitude smaller than the overall network conductivity.²⁸

Once the network has been reduced, we have evaluated σ by combining the numerical decimation algorithm of Ref. 29 with a preconditioned conjugated gradient method. Specifically, we decimated iteratively the network starting from the nodes with the lowest coordination number in order to eliminate dead ends and to compact the network. We continued the decimation procedure until a single conductance was left, whose value coincided with the conductance of the original network. If the computational time for the node decimation was too large, as it was typically the case for segregated sys-

tems with ϕ_1/v^* large, we switched to the conjugate gradient method (see e.g. Ref. 30) applied to the partially decimated network. We have applied this procedure to $N_r = 200 - 600$ realizations of systems with N_1 conducting spheres ranging from $N_1 = 250$ (for $L/D_1 = 50$ and $\phi_1 = 10^{-3}$) to $N_1 = 322690$ (for $L/D_1 = 80$ and $\phi_1 = 0.33$).

In Fig. 2 we show the distributions $P(\sigma)$ of the σ values obtained from 500 realizations of the system with $\phi_1 = 0.1$, $D_1/\xi = 50$, $D_2/D_1 = 8$, and for $\phi_2 = 0$ (with $L/D_1 = 25$), 0.4, and 0.6 (with $L/D_1 = 80$). All three sets of data follow approximately a log-normal distribution (solid lines) which stems from the exponential decay of Eq. (2) (note that the distribution of the $\phi_2 = 0$ case is broader than the two others because of the smaller size of L). The distributions are peaked at the average of the logarithm of σ , with no significant drifts when the system size is increased for fixed ϕ_1 . It is clear from the figure that, although ϕ_1 is kept fixed, the mean value of the conductivity steadily increases as the volume fraction ϕ_2 of the insulating spheres is enhanced. From Eq. (1) this trend can be interpreted by noticing that as ϕ_2 increases, the available volume fraction v^* decreases, so that the conducting particles occupy a reduced volume

compared to the homogeneous $\phi_2 = 0$ case (i.e., the effective concentration ϕ_1/v^* is larger). In turns this means that, as it can be inferred from Figs. 1(a) and (b), the mean interparticle distances δ_{ij} in Eq. (2) are reduced for $\phi_2 \neq 0$, thereby leading to an enhancement of the overall conductivity.

This behavior is clearly shown in Fig. 3, where we plot σ (symbols) as a function of ϕ_1 for $D_2/D_1 = 4$, Fig. 3(a), and $D_2/D_1 = 8$, Fig. 3(b), and for several values of the insulating sphere densities ϕ_2 . The reduction in σ for decreasing ϕ_1 , which is a direct consequence of the fact that as ϕ_1 is reduced the interparticle distances δ_{ij} get larger, can be strongly mitigated by the segregation which, through the reduction of v^* , tends instead to decrease δ_{ij} . We have therefore that, as shown in Fig. 3, for fixed values of the tunneling length ξ , as the segregation is enhanced the threshold value of ϕ_1 required to achieve a given σ decreases considerably. By combining this result with the observation that, in practice, the lowest measurable conductivity σ_{\min} in real composites is set either by the experimental setup or by the intrinsic conductivity of the insulating phase, and that this defines a sort of “critical” threshold ϕ_{1c} at which $\sigma \sim \sigma_{\min}$,¹⁶ we obtain that more segregated systems entail lower values of ϕ_{1c} . This last observation is in agreement with the behavior seen in real segregated composites if we reinterpret the percolation threshold values reported in the literature as our crossover concentration ϕ_{1c} .

As we shall see in the next section, the interpretation that the segregation basically leads to a shortening of the tunneling distances can be established on a firmer ground by employing the critical path approximation to the tunneling network. This analysis will also provides us with useful explicit formulas for the overall composite conductivity.

IV. CRITICAL PATH APPROXIMATION

We show in this section that, as for homogeneous dispersions of spherical, rod-like, and plate-like impenetrable particles,^{15,16} the critical path approximation (CPA) can also reproduce to a high accuracy the conductivity behavior for the inhomogeneous dispersions considered here. According to the CPA,²⁴ the composite conductivity σ can be expressed approximately as

$$\sigma = \sigma_0 \exp\left(-\frac{2}{\xi}\delta_c\right), \quad (3)$$

where $\delta_c \equiv \delta_c(\phi_1, \phi_2, D_2/D_1)$ is the largest among the δ_{ij} distances such that the sub-network defined by all distances $\delta_{ij} < \delta_c$ forms a conducting cluster spanning (or percolating) the entire sample. The critical distance δ_c defines the single bond critical conductance $g_c = \exp(-2\delta_c/\xi)$ which, once assigned to all the conductances g_{ij} of the network, leads to Eq. (3), where the prefactor σ_0 is the only remaining fitting parameter.

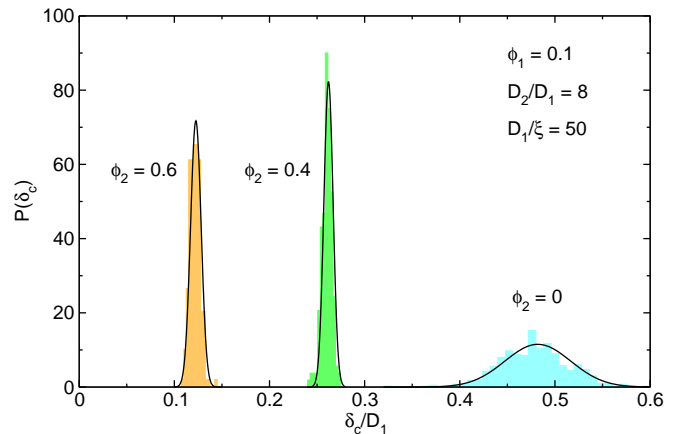


FIG. 4: (Color online) Histograms for the distribution $P(\delta)$ of the minimum interparticle distance δ required to have percolation for 500 realizations of the same systems considered in Fig. 2. The solid lines are fits to gaussian distribution functions.

Equation (3) reduces the conductivity problem to a simpler, geometrical one, which amounts to find the geometrical critical distance δ_c so that percolation is established. In practice, δ_c can be obtained by coating each conducting sphere by a concentric penetrable shell of thickness $\delta/2$ and by considering two spheres as connected if their shells overlap. The critical distance δ_c is then the minimum value of δ such that (for given values of ϕ_1 , ϕ_2 , and D_2/D_1) a cluster of connected spheres spans the sample. Hence, in contrast to the usual core-shell model approach to transport,^{4-7,11-13} here the shell thickness is not fixed *a priori* but it depends on the particle concentration.

Our numerical procedure to find δ_c goes as follows. For fixed volume fraction ϕ_1 of the conducting spheres, as well as for given ϕ_2 and D_2/D_1 values, we first generate the system as explained in Sec. II. For each realization i of the system ($i = 1, \dots, N_r$) we chose an initial value δ_i comprised within the interval $\Delta\delta = \delta_{\max} - \delta_{\min}$, where $\delta_{\min} = 0$ and δ_{\max} is large enough so that a percolating cluster is surely established. Clustering is performed on the adjacency list which represents the vicinity network. Namely, we scan iteratively the list by checking if a given node already belongs to previously classified clusters. If this condition is not fulfilled, we form a new cluster by identifying which nodes are directly and indirectly connected to the selected node. This is done by labeling the first and, recursively, the next levels in the vicinity hierarchy. Finally, a percolating cluster is the one in which at least two of its nodes lie at the opposite faces of the sample cube. The critical distance δ_c^i for the i -th realization is then found by bisecting the interval $\Delta\delta$ until convergence is reached within a relative error of 10^{-3} . Finally, an histogram representing the distribution $P(\delta_c)$ of the critical distance is obtained by repeating the procedure for all the N_r realizations of the system.

Examples of the thus obtained $P(\delta_c)$ are shown in Fig. 4 for the same cases of Fig. 2 (i.e., $\phi_1 = 0.1$, $D_2/D_1 = 8$, and $\phi_2 = 0, 0.4$, and 0.6). They approximately follow normal distributions (solid lines) centered at critical distances which steadily decrease as one moves from the homogeneous case ($\phi_2 = 0$) to the increasingly segregated regimes ($\phi_2 = 0.4$ and 0.6), thus confirming our previous conjecture that segregation implies a shortening of the tunneling lengths.

This trend is clearly seen in Fig. 5, where we plot the overall behavior of δ_c as a function of ϕ_1 and for different values of ϕ_2 and D_2/D_1 . At very low filler volume fractions, all δ_c curves for $\phi_2 \neq 0$ tend asymptotically to the critical distance of the homogeneous case (open circles) which in this limit behaves as $\delta_c \propto \phi_1^{-1/3}$, indicating that segregation is irrelevant for $\phi_1 \rightarrow 0$. As ϕ_1 increases, segregation acts by lowering the critical distance which, for large ϕ_2 and D_2/D_1 values, can be even one order of magnitude smaller than that of the homogeneous case.

The reduction of δ_c can be explained by using the argument that the available volume for placing the conducting spheres is reduced by segregation. Indeed, as Fig. 1(b) suggests, such a reduction has the net effect of increasing the local density of the D_1 particles, and so of reducing the critical distance for percolation. This argument neglects conductor-insulator interface effects and assumes that narrow bottlenecks are irrelevant for the establishment of the critical paths, which are conditions both fulfilled in the $D_2/D_1 \gg 1$ case.³¹

By following this line of reasoning, we argue that the only relevant variable for describing segregation is the available volume fraction v^* , and that consequently the critical distance can be expressed as $\delta_c(\phi_1, v^*)$. Furthermore, by requiring that the relevant ϕ_1 dependence of the D_1 particles is through the effective volume fraction ϕ_1/v^* , we express the critical distance as $\delta_c(\phi_1, v^*) = af(\phi_1/v^*)$, where $f(x)$ is a general function and a is a proportionality constant. The value of a can be determined by requiring that the critical distance for $\phi_1 \rightarrow 0$ coincides with that of the homogeneous case, which leads us to the following scaling relation

$$\delta_c(\phi_1, v^*) = v^{*-1/3} f(\phi_1/v^*). \quad (4)$$

As shown in the insets of Fig. 5, where $v^{*1/3}\delta_c$ is plotted as a function of ϕ_1/v^* , the data for different ϕ_2 values basically collapse into a single curve already for $D_2/D_1 \geq 8$. However, for $D_2/D_1 = 4$ the scaling relation (4) is not very effective but, as shown in the Appendix, the scaling argument can be generalized in order to provide a better data collapse also for $D_2/D_1 < 8$.

From the scaling relation (4) it follows that for $v^* = 1$ the function $f(\phi_1)$ coincides with the critical distance in the homogeneous limit $\delta_c(\phi_1, 1)$, thereby leading to

$$\delta_c(\phi_1, v^*) = v^{*-1/3} \delta_c(\phi_1/v^*, 1), \quad (5)$$

which merely states that the critical distance in the segregated regime can be directly obtained from that of the homogeneous case. In order to illustrate the consequences

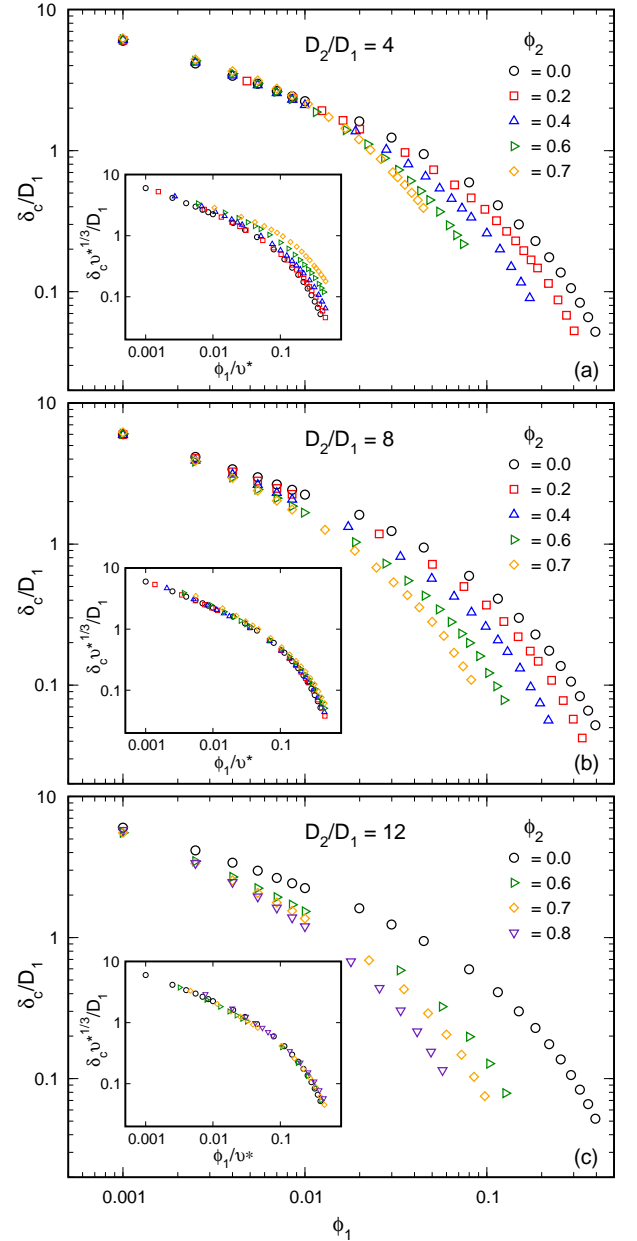


FIG. 5: (Color online) Critical distance δ_c dependence on the volume fraction ϕ_1 of the conducting D_1 spheres for several values ϕ_2 of the volume fraction of the insulating D_2 spheres for (a) $D_2/D_1 = 4$, (b) $D_2/D_1 = 8$, and (c) $D_2/D_1 = 12$. Insets: the same data plotted according to the scaling relation of Eq. (4).

of Eq. (5) for the conductivity σ of segregated composites, let us first verify that the CPA of Eq. (3) actually provides a valuable approximation of σ . In Fig. 6 we replot the conductivity data of Fig. 3 as a function of the critical distance results of Fig. 5. Irrespectively of ϕ_2 and of D_2/D_1 , we find that σ nicely follows the linear relation

$$\ln(\sigma) = \ln(\sigma_0) - \frac{2}{\xi} \delta_c, \quad (6)$$

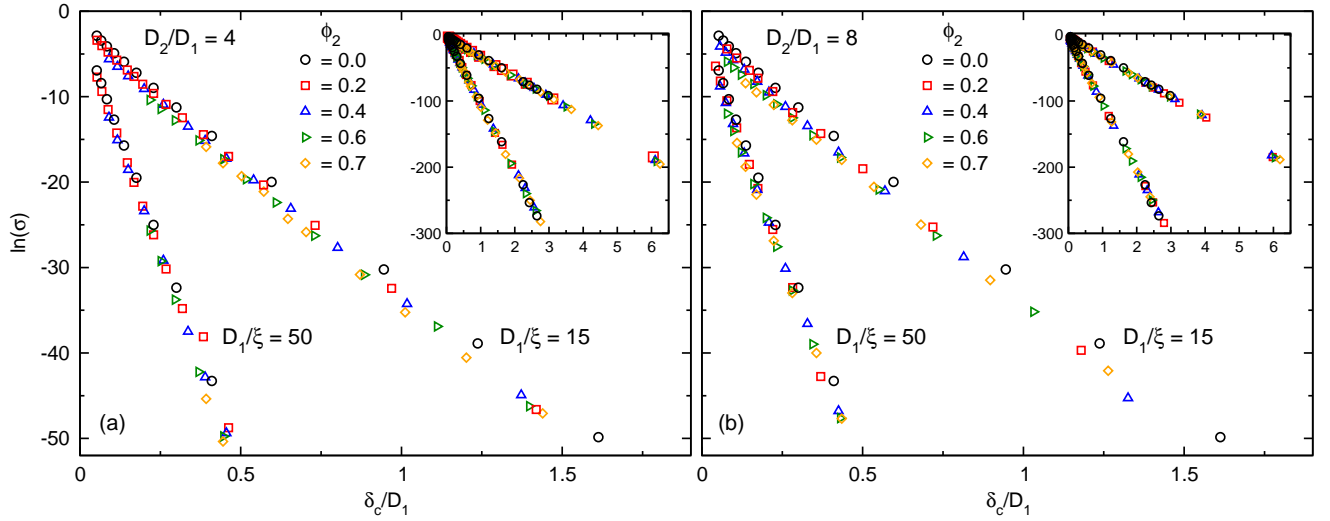


FIG. 6: (Color online) Natural logarithm of the conductivity values σ of Fig. 3 plotted as a function of the critical distance δ_c of Fig. 5. (a) $D_2/D_1 = 4$; (b) $D_2/D_1 = 8$. The insets show the $\ln(\sigma)$ versus δ_c/D_1 dependence in a larger scale.

with slope $2/\xi$, and that therefore the CPA is in excellent agreement with the full numerical solution of the tunneling resistor network. Thus, from Eqs. (3) and (5), this means that for $D_2/D_1 \gg 1$ (see the Appendix for the $D_2/D_1 \sim 1$ case) we can express σ in terms of the critical distance $\delta_c(\phi_1, 1)$ of the homogeneous limit, leaving only the prefactor σ_0 to be determined. By using some approximate formula for $\delta_c(\phi_1, 1)$, like for example those reported in Refs. 15,16,35, the full ϕ_1 dependence of σ for given v^* can be then expressed in analytical terms with high accuracy. This is illustrated in Fig. 3(b), where the solid lines have been obtained from

$$\sigma = \sigma_0 \exp \left[-\frac{2 \delta_c(\phi_1/v^*, 1)}{\xi v^{1/3}} \right], \quad (7)$$

with v^* from Eq. (1), $D_2/D_1 = 8$, and $\delta_c(x, 1)$ as given in Ref. 15.³⁶ As shown in the next section, the possibility of expressing the composite conductivity in terms of an analytic formula is a valuable tool to describe the filler dependences of real segregated composites and to interpret the experimental data.

V. APPLICATION TO EXPERIMENTS

We show here that the result of the previous section can be used to analyze experimental σ vs ϕ_1 data in order to extract estimates of the tunneling length ξ value and of the degree of segregation in the composite. This is so because, if the experimental values of $\ln(\sigma)$ are plotted as a function of δ_c instead of ϕ_1 , and if our GTN picture applies, then they are expected to follow Eq. (6) whose slope $-2/\xi$ directly gives the value of the tunneling factor ξ independently of the specific σ_0 value. Furthermore, the available volume fraction v^* appearing in Eq. (5) does

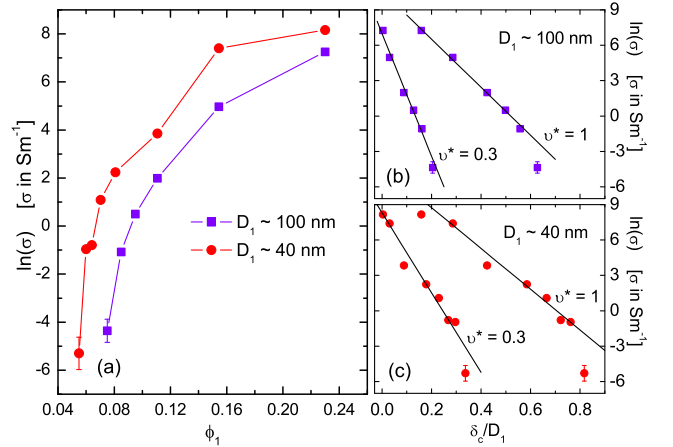


FIG. 7: (Color online) (a) Experimental conductivity σ data of two series of RuO₂-cermets as a function of the volume fraction ϕ_1 of the RuO₂ particles (from Ref. 32). The same σ values are plotted as a function of the critical distance δ_c for (a) $D_1 \sim 100$ nm and (c) $D_1 \sim 40$ nm by assuming two different values of the available volume fraction v^* . The solid lines are fits to Eq. (6).

not depend, in principle, on the particular model chosen to represent segregation,³⁷ and so it may be used as a fitting parameter which best reproduces the experimental data.

In order to illustrate how the theory applies to real composites, we consider here the conductivity data of RuO₂-cermet samples which were already reported in Ref. 32. In particular we consider two series of samples constituted by RuO₂ conducting particles of mean sizes $D_1 \approx 40$ nm and $D_1 \approx 100$ nm, dispersed in a borosilicate glass. The glassy grains prior to thermal processing

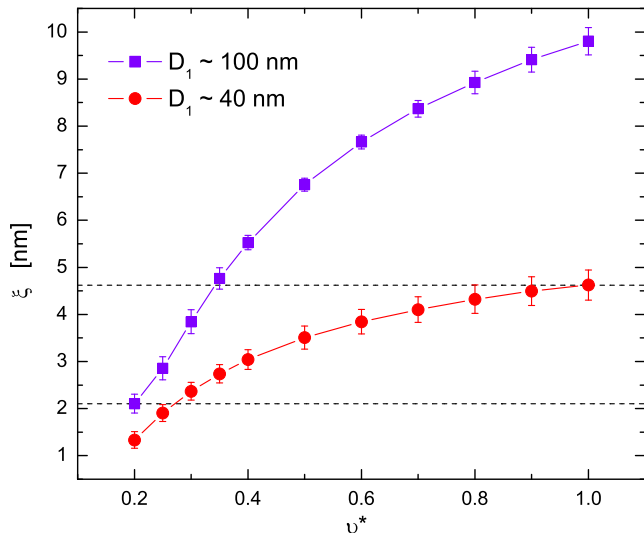


FIG. 8: (Color online) Values of the tunneling decay distance ξ as a function of the available volume fraction v^* extracted as explained in the text. The two horizontal dashed lines at 4.6 nm and 2.1 nm represent the maximum and minimum values of ξ which are compatible with both series of composites.

(firing) had average size of about $3\mu\text{m}$, so that for both series of composites $D_2/D_1 \gg 1$. The two series of samples were fired by following identical thermal cycles so that, in principle, they differ only in the mean size D_1 of the conducting RuO_2 particles. It should be noted however that although the finer RuO_2 powders were given by nearly spherical and monodispersed particles, the coarser powders had more dispersed grain sizes with less regular shape.

In Fig. 7(a) we plot the measured conductivity as a function of RuO_2 volume fraction ϕ_1 for both series of composites. In Ref. 32 we interpreted these same data in the framework of percolation theory and fitted them with the power-law relation $(\phi_1 - \phi_{1c})^t$. The resulting low percolation threshold values, $\phi_{1c} \simeq 0.07 - 0.05$, were found to be consistent with the segregated distribution of the RuO_2 conducting phase observed in the microstructure, while the large transport exponent values, $t \simeq 3 - 4$, were concluded to arise from the nonuniversality of the critical behavior as predicted by the tunneling-percolation model of Ref. 33 (see also later developments of this theory in Refs. 31,34). Here, we offer an alternative interpretation of these data based on the GTN theory which, as explained in this paper and in Refs. 15–17, is more justified on physical grounds than our previous percolation-based one of Ref 32.

Let us start by re-plotting the conductivity data of Fig. 7(a) in terms of the critical distance $\delta_c(\phi_1, v^*)$ by using the scaling relation of Eq. (5). For the functional form of $\delta_c(\phi_1/v^*, 1)$ we use the fitting formula published in Ref. 15,³⁶ and we treat v^* as an adjustable parameter.³⁸ The resulting $\ln(\sigma)$ vs δ_c plots for two different values of

v^* are shown in Fig. 7(b) and Fig. 7(c) for the $D_1 \approx 100$ nm and $D_1 \approx 40$ nm samples, respectively. In both cases the data follow a better linear dependence for $v^* = 0.3$ (strong segregation) than for $v^* = 1$ (homogeneity), and from the corresponding fits to Eq. (6) (solid lines) we obtain that lower values of v^* imply also lower values of ξ (i.e., the slopes are larger). This is most clearly seen in Fig. 8 where we report the v^* dependence of the so-obtained ξ values for both series of samples. Starting from the homogeneous limit at $v^* = 1$ the tunneling length ξ of the $D_1 \approx 100$ nm series decreases by a factor of five when the available volume fraction is lowered down to the minimum value $v^* = 0.2$ for which a linear fit of $\ln(\sigma)$ vs δ_c was possible, while the $D_1 \approx 40$ nm case displays a weaker decrease in the same range of v^* due to the smaller RuO_2 grain size. By realizing that the tunneling decay length should be independent of the size D_1 of the conducting particles, while the specific v^* value could be different for the two series of composites, then ξ must be comprised between the two horizontal dashed lines at 4.6 nm and 2.1 nm in Fig. 8. However, since the microstructure of both series of composites displays a marked segregated dispersion,³² then v^* should be sensibly smaller than the unity, suggesting that the lower limit $\xi \simeq 2$ nm is a more reliable estimate for ξ . This value is fully comparable to those extracted from other conductor-insulator composites,^{15,16} and, specifically, agrees well with the results of microscopical investigations of thick-film cermet resistors.³⁹

VI. CONCLUSIONS

In this paper we have generalized the GTN model, where each conducting particle is connected to all others through tunneling processes, to describe composites whose microstructure is given by a segregated dispersion of the conducting phase. This particular class of non-homogeneous composites is characterized by large conductivity even for volume fraction values ϕ_1 of the conducting phase as low as a few percents. According to the percolation theory, this behavior is explained by the reduced values of the percolation threshold induced by the segregated dispersion of the conducting particles. Here, we have shown that the ϕ_1 dependence of the conductivity in nonhomogeneous segregated composites can be understood without imposing any fixed cut-off in the microscopic electrical connectivity (as it is done in percolation theory) and that the GTN formulation provides thus a natural and physically justified approach to the study of transport in disordered composites.

Besides the full numerical solutions of the tunneling resistor network, we have also shown that the critical path approximation is valid for a wide range of ϕ_1 , and that it permits to formulate a scaling relation connecting the critical tunneling distance δ_c for a segregated systems with that of a homogeneous composite. Finally, we have illustrated the practical importance of this scal-

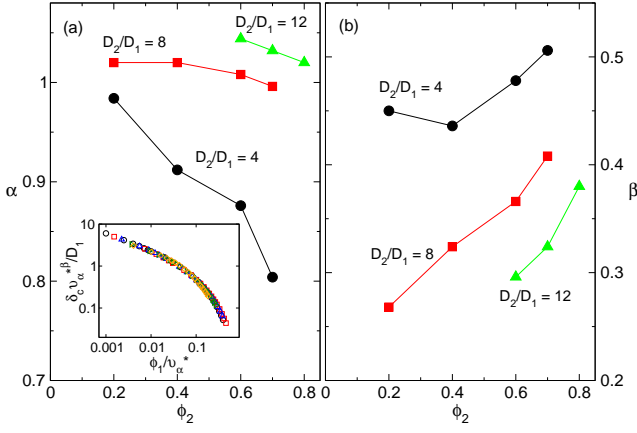


FIG. 9: (Color online) Dependence of the correction parameter (a) α and (b) β on the volume fraction ϕ_2 of the insulating spheres and on D_2/D_1 . Inset: the δ_c data for $D_2/D_1 = 4$ of Fig. 5(b) rescaled according to Eq. (A2) for the corresponding values of α and β .

ing by applying it to experimental conductivity data of RuO₂-cermet segregated composites, which has permitted us to extract a realistic tunneling decay length ξ and to estimate the degree of segregation in these materials.

Acknowledgments

This work was supported by the Swiss National Science Foundation (Grant No. 200021-121740).

Appendix A: improved scaling formula

Here we briefly address the problem of generalizing the scaling relation of Eq. (5) in order to extend its validity beyond the $D_2/D_1 \gg 1$ regime. To this end, let us first remind that v^* defined in Eq. (1) gives the volume fraction available for placing the centers of the conducting

particles with diameter D_1 . However, in order to define the critical distance δ_c , the conducting spheres are treated as core-shell particles, where the hard-core of diameter D_1 is coated by a concentric penetrable shell of thickness $\delta_c/2$. Since this penetrable shell may actually overlap the insulating spheres then, to what concerns the connectivity, these latter may be treated as having effectively a smaller diameter $\alpha D_2 \leq D_2$, where $0 \leq \alpha \leq 1$ is a correction factor which captures such effective reduction. In this way the corrected available volume fraction reads:

$$v_\alpha^* = (1 - \phi_2)^{(\alpha + D_1/D_2)^3}. \quad (\text{A1})$$

For $\alpha \leq 1$ the net effect of the overlapping between shells and insulating spheres is then an effective increase of the available volume. This increase is expected to be unimportant when $D_2/D_1 \gg 1$, so that $\alpha \simeq 1$ in this regime, while when the two diameters D_1 and D_2 are comparable the α correction has to be considered. By using Eq. (A1), we generalize thus the scaling relation (4) as follows:

$$\delta_c(\phi_1, v_\alpha^*) = v_\alpha^{*- \beta} f(\phi_1/v_\alpha^*), \quad (\text{A2})$$

where in addition to the corrected available volume v_α^* we have introduced the new exponent β to improve the scaling in the large ϕ_1 region.

In Fig. 9 we plot (a) α and (b) β obtained from the minimization of $||\delta_c(\phi_1/v_\alpha^*, 1) - v_\alpha^{*- \beta} \delta_c||$ as functions of the volume fraction ϕ_2 of the insulating spheres and for $D_2/D_1 = 4, 8$, and 12 . For $D_2/D_1 = 8$ and 12 the coefficients α and β are close to respectively $\alpha = 1$ and $\beta = 1/3$ for all values of ϕ_2 considered, so that, as expected, Eq. (5) with v^* as given in Eq. (1) provides a rather good scaling of the δ_c data. On the contrary, for $D_2/D_1 = 4$ the coefficient α displays a stronger ϕ_2 dependence and is sensibly smaller than $\alpha = 1$ for large ϕ_2 values, while β is larger than $1/3$. In particular, $\alpha < 1$ indicates that for this case the increase of the effective available volume v_α^* is an important effect for the correct scaling of δ_c which, as shown in the inset of Fig. 9(a), is now almost perfect.

* Electronic address: biagio.nigro@epfl.ch

† Electronic address: claudio.grimaldi@epfl.ch

¹ C. -W. Nan, Y. Shen, and J. Ma, *Annu. Rev. Mater. Res.* **40**, 131 (2010).

² T. Schilling, S. Jungblut, and M. A. Miller, *Networks of Nanorods*, in *Handbook of Nanophysics: Nanotubes and Nanowires*, Ed. K. D. Sattler (Taylor & Francis, New York, 2010).

³ T. Tamai, *IEEE T. Compon. Hybr.* **5**, 56 (1982); R. Strümpfer and J. Glatz-Reichenbach, *J. Electroceram.* **3**, 329 (1999); D. D. L. Chung, *J. Mater. Sci.* **39**, 2645 (2004); R. N. Torah, S. P. Beeby, M. J. Tudor, and N. M. White, *J. Electroceram.* **19** 95 (2007);

⁴ J. F. Wang and A. A. Ogale, *Compos. Sci. Technol.* **46**, 93

(1993).

⁵ X. Jing, W. Zhao, and L. Lan, *J. Mater. Sci. Lett.* **19**, 377 (2000).

⁶ D. He and N. N. Ekere, *J. Phys. D: Appl. Phys.* **37**, 1848 (2004).

⁷ L. Berhan and A. M. Sastry, *Phys. Rev. E* **75**, 041120 (2007).

⁸ D. Stauffer and A. Aharony, *Introduction to Percolation Theory* (Taylor & Francis, London, 1994).

⁹ M. Sahimi, *Heterogeneous Materials I. Linear Transport and Optical Properties* (Springer, New York, 2003).

¹⁰ I. Balberg, C. H. Anderson, S. Alexander, and N. Wagner, *Phys. Rev. B* **30**, 3933 (1984); I. Balberg and N. Binenbaum, *Phys. Rev. A* **35**, 5174 (1987).

- ¹¹ T. Schilling, S. Jungblut, and M. A. Miller, Phys. Rev. Lett. **98**, 108303 (2007).
- ¹² A. V. Kyrylyuk and P. van der Schoot, Proc. Natl. Acad. Sci. USA **105**, 8221 (2008).
- ¹³ R. H. J. Otten and P. van der Schoot, Phys. Rev. Lett. **103**, 225704 (2009).
- ¹⁴ I. Balberg, J. Phys. D: Appl. Phys. **42**, 064003 (2009).
- ¹⁵ G. Ambrosetti, N. Johner, C. Grimaldi, T. Maeder, P. Ryser, and A. Danani, J. Appl. Phys. **106**, 016103 (2009).
- ¹⁶ G. Ambrosetti, C. Grimaldi, I. Balberg, T. Maeder, A. Danani, and P. Ryser, Phys. Rev. B **81**, 155434 (2010).
- ¹⁷ G. Ambrosetti, I. Balberg, and C. Grimaldi, Phys. Rev. B **82**, 134201 (2010).
- ¹⁸ R. P. Kusy, J. Appl. Phys. **48**, 5301 (1977).
- ¹⁹ N. Johner, C. Grimaldi, T. Maeder, and P. Ryser, Phys. Rev. E **79**, 020104(R) (2009).
- ²⁰ G. E. Pike and C. H. Seager, J. Appl. Phys. **48**, 5152 (1977); P. F. Carcia, A. Ferretti, and A. Suna, J. Appl. Phys. **53**, 5282 (1982); A. Kusy, Physica B **240**, 226 (1997); A. Alessandrini, G. Valdrè, B. Morten, and M. Prudenziati, J. Appl. Phys. **92**, 4705 (2002).
- ²¹ A. Malliaris and D. T. Turner, J. Appl. Phys. **42**, 614 (1971).
- ²² Y. P. Mamunya, V. V. Davydenko, P. Pissis, and E. V. Lebedev, Eur. Polym. J. **38**, 1887 (2002).
- ²³ G. E. Pike, in *Electrical Transport and Optical Properties of Inhomogeneous Media*, edited by J. C. Garland and D. B. Tanner (Americal Institue of Physics, New York, 1978), p.366; A. Kubový, J. Phys. D: Appl. Phys. **19**, 2171 (1986); I. J. Youngs, J. Phys. D: Appl. Phys. **36**, 738 (2003); N. Lebovka, M. Lisunova, Ye P. Mamunya, and N. Vygornitskii, J. Phys. D: Appl. Phys. **39**, 2264 (2006); W. J. Kim, M. Taya, K. Yamada, and N. Kamiya, J. Appl. Phys. **83**, 2593 (1998).
- ²⁴ V. Ambegaokar, B. I. Halperin, and J. S. Langer, Phys. Rev. B **4**, 2612 (1971); M. Pollak, J. Non Cryst. Solids **11**, 1 (1972); B. I. Shklovskii and A. L. Efros, Sov. Phys. JETP **33**, 468 (1971); **34**, 1084 (1972). C. H. Seager and G. E. Pike, Phys. Rev. B **10**, 1435 (1974); H. Overhof and P. Thomas, *Hydrogetaned Amorphous Semiconductors* (Springer, Berlin, 1989).
- ²⁵ S. Torquato, *Random Heterogeneous Materials: Microstructure and Macroscopic Properties* (Springer, New York, 2002).
- ²⁶ J. D. Sherwood, J. Phys. A **30**, L839 (1997).
- ²⁷ G. Li, L. A. Braunstein, S. V. Buldyrev, S. Havlin, and H. E. Stanley, Phys. Rev. E **75**, 045103(R) (2007).
- ²⁸ Specifically, we have first evaluated the critical bond conductance $g_c = \exp(-2\delta_c/\xi)$ resulting from the critical path approximation described in Sec. IV. Next, we have chosen δ^* in order to satisfy $\exp(-2\delta^*/\xi) = \exp(-M)g_c$, where $M = 20, 10, 5$ for $g_c < 10^{-50}$, $10^{-50} < g_c < 10^{-10}$, and $10^{-10} < g_c$, respectively.
- ²⁹ R. Fogelholm, J. Phys. C **13**, L571 (1980).
- ³⁰ G. G. Batrouni and A. Hansen, J. Stat. Phys. **52**, 747 (1988).
- ³¹ N. Johner, C. Grimaldi, I. Balberg, and P. Ryser, Phys. Rev. B **77**, 174204 (2008).
- ³² S. Vionnet-Menot, C. Grimaldi, T. Maeder, S. Strässler, and P. Ryser, Phys. Rev. B **71**, 064201 (2005).
- ³³ I. Balberg, Phys. Rev. Lett. **59**, 1305 (1987).
- ³⁴ C. Grimaldi and I. Balberg, Phys. Rev. Lett. **96**, 066602 (2006).
- ³⁵ D. M. Heyes, M. Cass, and A. C. Brańca, Mol. Phys. **104**, 3137 (2006).
- ³⁶ Note that in the expression for $\delta_c(x,1)$ given in Ref. 15 there is a factor 2 missing. The correct expression is: $\delta_c(x,1) = 2/[A_0 + A_1 \exp(x/t_1) + A_2 \exp(x/t_2)]$, with $A_0 = -7.33$, $A_1 = 7.25$, $A_2 = 0.81$, $t_1 = 0.355$, and $t_2 = 0.114$.
- ³⁷ Indeed, the concept of available volume fraction is very general, and it can be applied also to dispersions of insulating objects which are non-spherical, polydispersed, partially or completely impenetrable.
- ³⁸ Since the larger RuO₂ volume fraction value in Fig. 7(a) is $\phi_1 = 0.23$, for $v^* < 0.36$ the effective concentration ϕ_1/v^* becomes larger than the random close-packed limit $\simeq 0.64$. Hence, in order to maintain consistency with our formulation, we have considered in the fitting for $v^* < 0.4$ only the low density data of Fig. 7(a).
- ³⁹ Y.-M. Chiang, L. A. Silverman, R. H. Freanch, and R. M. Cannon, J. Am. Ceram. Soc. **77**, 1143 (1994).